A Unified Circuit Model for Ferroelectrics

Kshitij Auluck*, Edwin C. Kan
School of Electrical and Computer Engineering
Cornell University, Ithaca, NY, USA
*ka323[at]cornell.edu

Shantanu R. Rajwade
Intel Corporation, Santa Clara, CA, USA

***Abstract*—We present a physical circuit model for polarization reversal dynamics in ferroelectrics, which is implemented in Verilog-A, validated with PZT measurements and applicable in all operation modes for bulk, epitaxial and polycrystalline thin films. Consistent treatment of field-driven polarization not only gives accurate step-voltage responses across many decades in time, but also reproduces frequency and amplitude dependent P-E and I-V hysteresis loops for ferroelectric MIM capacitors. FE-RAM and gate-stack FE-FET circuit simulations are experimentally verified.**

Keywords—ferroelectric; compact model; FE-FET; PZT

I. INTRODUCTION

The demand for ultra-low power computing has generated interest in nonvolatile embedded systems [1] and check-pointing architectures [2], which can retain the state of computation under uncertain power availability. Ferroelectric (FE) circuits are attractive for these applications due to their low-power, low-voltage operation and maturity in the CMOS fabrication. Novel FE-RAM sensing schemes [3], FE-FET latches [4] and FE DFFs [1], have been recently demonstrated. Analog circuits that exploit the unique energy storage and nonlinear characteristics of FE, such as switched FE-capacitor DC-DC converters [5], have also been proposed.

Analysis, design optimization and benchmarking of complex circuits with FE elements requires unified, C-∞ and computationally efficient compact models. Although recent works have provided direct experimental insights into the physics of polarization switching kinetics [6-8], present circuit CAD models [9-11] are valid only for specific regions of operation and cannot be universally applied to arbitrary inputs (e.g. low voltages) or device geometries (e.g. FE-FET transients). FE compact models must also take material and geometric input parameters for device-circuit co-design and simulation of fatigue and imprint effects on circuit performance.

We review the physics of domain switching in Section II and derive the circuit model in Section III. Experimental validation and parameter extraction are presented in Section IV, followed by FE-RAM and FE-FET circuit simulation and measurements in Section V. Comparison with present circuit models is discussed in Section VI.

II. PHYSICS OF POLARIZATION SWITCHING

Electric field driven domain switching is a first-order phase transition and proceeds by nucleation and growth of opposite domains. From a fully poled state, switching is initiated by formation of needle-shaped nuclei originating at the electrodes [12], which propagate forward to reach the opposite electrode. The rate limiting step in polarization response is the sideways growth and coalescence of the through-domains to fill the FE volume.

A. Sideways growth and domain coalescence

Sideways domain wall velocity at an applied electric field $E_{Applied}$ depends on structural properties such as polarization rotation and strain. In the thermally activated regime, critical nuclei are formed on the domain wall with free energy change U_{nucl} and characteristic nucleation time τ, assisted by thermal fluctuations. U_{nucl} is obtained by minimizing the sum of the electrostatic, surface and depolarization energies as a function of nucleus dimensions, and has a power-law dependence on $E_{Applied}$ [13].

$$\tau = \tau_0 \, exp\left(\frac{U_{nucl}}{kT}\right) = \tau_0 \, exp\left(\frac{E_a}{E_{Applied}}\right)^n \quad (1)$$

The attempt rate τ_0 is the inverse soft-phonon frequency and E_a is the activation field. In non-thermally activated switching, domain wall velocity is obtained from the time-dependent Landau-Ginzburg equation and has linear electric field dependence [14].

Assuming large number of randomly distributed nuclei, the switched polarization $\triangle p(t)$ is given by the statistics of domain coalescence from the Kolmogorov-Avrami-Ishibashi (KAI) theory [15].

$$\triangle p(t) = 2 P_r \left(1 - exp\left(-\left(\frac{t}{\tau(E_{Applied})}\right)^m\right)\right) \quad (2)$$

Here, the Avrami exponent m denotes the dimensionality of domain growth for site-saturated and continuous nucleation mechanisms [16], $\tau(E_{Applied})$ is obtained from Eq. (1) and P_r is the remanent polarization experimentally measured from the Positive-Up-Negative-Down (PUND) technique [17] or hysteresis loops.

B. Deviation from the KAI theory

The KAI theory matches bulk and epitaxial FE polarization transients well, but has significant deviation for disordered polycrystalline FE at low voltages [17]. Time-resolved piezo-response force microscopy indicated retardation in domain wall velocity with coalescence [18]. This effect has been attributed to non-idealities such as defects and interfaces, both of which

can be treated by adding correction terms to the applied field to obtain an effective field, E_{FE}, for domain wall motion (Eq. 3).

$$E_{FE}(t) = E_{Applied} + E_{Correction}(t) \quad (3)$$

The role of dipole defects has been treated by adding a stochastic field with Lorentzian distribution to the applied field [19]. The correction field for interface effects such as charged domain walls, grain boundaries, Schottky barrier and intrinsic dead layer, is the depolarization field, which acts as a negative feedback to the applied field (Eq. 4) [20].

$$E_{FE}(t) = E_{Applied} - \frac{p(t)}{d_{FE}(C_{el}+C_{dead})} \quad (4)$$

where $p(t)$ is the polarization, d_{FE} is the FE film thickness, C_{el} is the capacitance corresponding to the electronic polarization of FE. The combined effect of interfaces is lumped into the dead-layer capacitance C_{dead}.

C. Equilibrium polarization

To obtain the field-dependent polarization state in the asymptotic limit of t=∞, the film is treated as an ensemble of elementary regions with volume v equal to the critical nucleus. The free energy of each region has two local minima corresponding to the stable polarization states, separated by the electrostatic energy $2P_S E_{FE} v$, where P_S is the unit-cell polarization of the FE. From Boltzmann statistics, the equilibrium polarization can be estimated as $P_{eq} = P_r tanh(\frac{P_S E_{FE} v}{kT})$ [21]. Substituting P_r by P_{eq} in Eq. (2), we get

$$\frac{dp}{dt} = \frac{P_{eq}-p}{\tau(E_{FE})}\left(\frac{t}{\tau(E_{FE})}\right)^{m-1} \quad (5)$$

where $E_{FE}(t)$ is given by Eq. (4). Since critical nucleus volume is on the order of 10^{-19} cm^3 [22], the equilibrium polarization $P_{eq}(E_{FE}) \approx \pm P_r$, for $|E_{FE}|$ > 10 kV/cm.

D. Defect domain-wall interaction

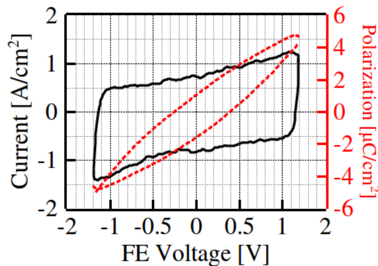

Fig. 1. Sub-coercive current (solid) and polarization loops (dashed) at 50 kHz (experiments) show an irreversible component of polarization when the applied voltage is recovered.

Weakly pinned domain walls can jump over the local potential barriers from defects which gives rise to Rayleigh hysteresis loops [23] at sub-coercive fields:

$$p_d(t) = \epsilon_0(\gamma E_m E_{FE}(t) \pm \frac{\gamma}{2}(E_m^2 - E_{FE}(t)^2)) \quad (6)$$

where p_d is the polarization due to defect domain-wall interaction, Rayleigh coefficient γ is proportional to the defect density in the FE, and E_m is the maximum sub-coercive field applied to the FE. The displacement current density normalized to the ramp rate increases linearly with the applied field (Fig. 1), clearly showing some irreversible polarization in the hysteresis loop.

III. Circuit Model

When the domain growth dimensionality m = 1, Eq. (5) from the KAI theory resembles the current response of a RC circuit (Fig. 2) with voltage-controlled voltage source **V1** = $kP_{eq}(V_{FE})$ which represents the thermodynamic potential driving the domain walls towards equilibrium. Here k is a normalization constant. The time constant for domain coalescence is the field-dependent nucleation time in Eq. (1), which is represented by the voltage-dependent resistor **R1** = $k\,\tau(V_{FE})$. For $m\neq$ 1, the time-integral function (`idt`) is used to implement Eq. (5), instead of resistor **R1**.

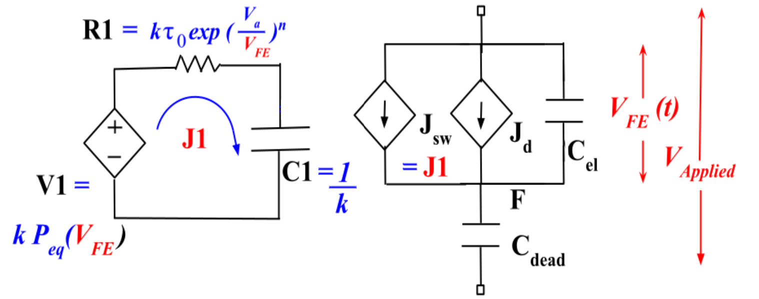

Fig. 2. The domain switching current is modeled by $\mathbf{J_{sw}}$which is equal to the current **J1** in the RC circuit for Avrami exponent m=1. The displacement current due to defect-domain wall interaction is $\mathbf{J_d}$. Dead layer capacitance $\mathbf{C_{dead}}$ provides negative feedback for inhomogeneous switching. $\mathbf{C_{el}}$ represents FE electronic polarization.

The correction field which models the retardation of domain wall velocity due to interfaces is proportional to the polarization $p(t)$ in the first order in Eq. (4). This can be implemented by placing charge on the floating node between a constant capacitance $\mathbf{C_{dead}}$ in series with $\mathbf{C_{el}}$ to obtain $V_{FE}(t)$.

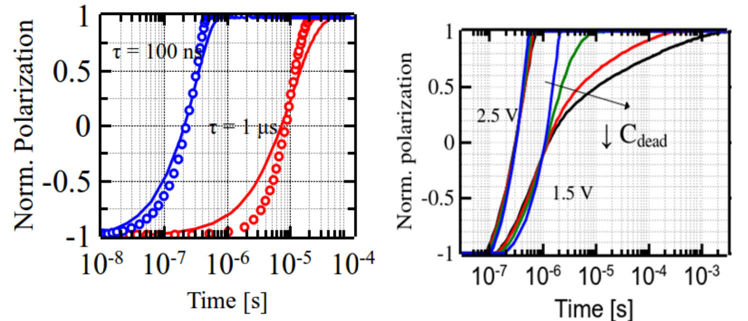

Fig. 3. a) In bulk/epitaxial FE, Avrami exponent m=2 (circles) shows steeper response than m=1 (solid). b) In thin-film FE, decreasing the dead layer capacitance stretches the polarization response.

The dependent current source $\mathbf{J_{sw}}$ is equal to the current **J1** in the RC circuit and represents the domain switching current

from Eq. (5). Non-switching polarization current due to defect domain-wall interaction from Eq. (6) is given by the dependent current source $\mathbf{J_d} = \epsilon_0 \gamma (E_m \mp E_{FE}) \frac{d\,E_{FE}}{d\,t}$.

Notice that FE polarization, which is memorized on the floating node **F**, evolves self-consistently as time integral of $\mathbf{J_{sw}}$+ $\mathbf{J_d}$. Charge conservation is guaranteed since polarization switching is self-limited when the charge on **F** reaches the equilibrium state. Energy conservation holds because energy is stored and dissipated, but never generated in the FE branch.

Fig. 3a shows simulation by Cadence Spectre, highlighting the effects of KAI parameters for bulk/epitaxial FE which do not show the retardation effect. This is treated with $\mathbf{C_{dead}}$ >> $\mathbf{C_{el}}$. Increasing τ will lead to a parallel shift in logarithmic time, and increasing m will lead to sharpening of the polarization transient. For disordered FE, decreasing $\mathbf{C_{dead}}$ will skew the polarization response (Fig. 3b), leading to high retardation of domain wall motion at low fields.

IV. Parameter Extraction

Device parameters were extracted from Pt-PZT-Pt MIM capacitors from Radiant Technology, with 140 nm thick 3% Nb-doped tetragonal $PbZr_{0.2}Ti_{0.8}O_3$. Switching polarization transient response from step-voltage input is obtained from the PUND technique [17]. Current-voltage (I-V) loops were obtained by applying triangular voltage waveforms and measuring the displacement current by Keithley 4200 SCS. Rayleigh coefficient γ is extracted from sub-coercive I-V loops in Fig. 1 without significant frequency dependence till 500 kHz.

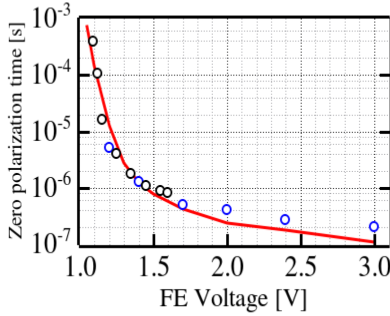

Fig. 4. Time required for zero polarization from the fully poled state as a function of voltage pulse amplitude. Circles: experiment; solid: model.

Notice that our model predicts large dependence on $\mathbf{C_{dead}}$ in switching polarization transients only at high positive switched polarization (Fig. 3b), when the feedback field term in Eq. (4) is comparable to the applied field. Therefore, nucleation rate parameters τ_0, E_a and n can be extracted by fitting the zero-polarization crossing time of PUND transients as a function of the voltage step height (Fig. 4). By setting τ_0= 10^{-13}s according to the PZT soft-phonon frequency, the best match was obtained for n=1.5. Using the extracted nucleation parameters, the complete polarization transients were matched with simulations (Fig. 5) to extract $\mathbf{C_{dead}}$.

Extracted FE parameters are shown in Table I. Experiments for varying amplitudes of the triangular input voltage match well with simulations (Fig. 7a). P-E loops can be matched for a wide range (500 Hz–200 kHz) of frequencies (Fig. 7b).

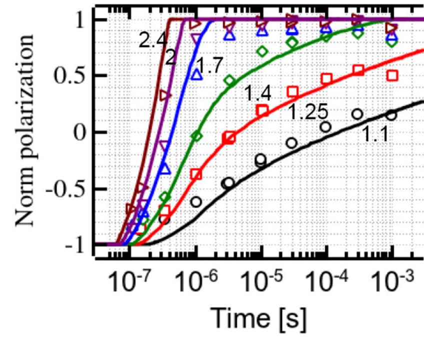

Fig. 5. Polarization response at varying step heights (V) in experiment (circles) and simulation (solid).

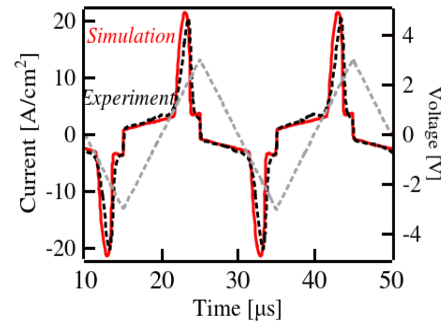

Fig. 6. For triangular applied voltages, the displacement current density peaks at the coercive field (switching current) and is linear at sub-coercive fields (non-switching current).

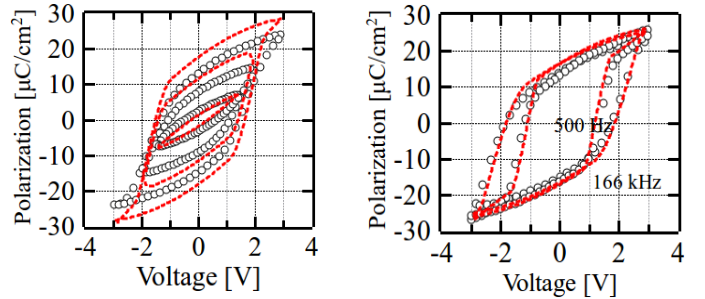

Fig. 7. a) Simulated (dashed) and measured (circles) P-E hysteresis sub-loops at 50 kHz. b) Simulated (dashed) and measured (circles) P-E hysteresis loops at 500 Hz and 166 kHz.

V. Circuit Simulation

The FE-RAM circuit was implemented with discrete transistors from ALD 1105 chip. Bit-line, word-line and plate-line signals (2.5 V) were applied from Altera DE-2 FPGA board. Circuit simulation and measurements for bitline waveforms are compared in write and read operations for bit 1 and bit 0 (Fig. 8).

Program/erase (P/E), disturb and retention operations in FE-FET cause domain switching kinetics across vastly different time scales. For example, P/E time is typically < 100 ns, while retention time is on the order of days. Further, FE electric fields in all operations are time-dependent, due to negative feedback from polarization. Memory window transient simulations for $Si/HfO_2/PZT/SiO_2/Pt$ FE-FETs compared well with our fabricated devices [24] (Fig. 9).

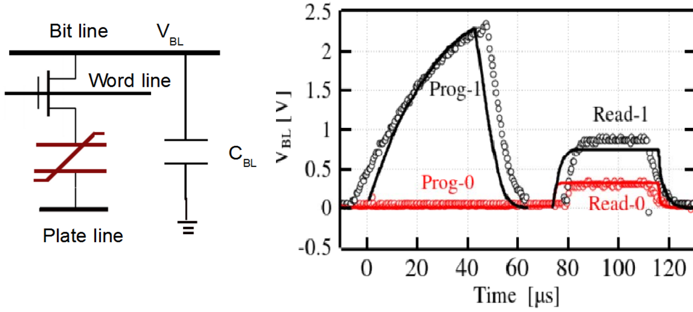

Fig. 8. Simulated (solid) and measured (circles) bit line voltage waveforms for FE-RAM program and read operations.

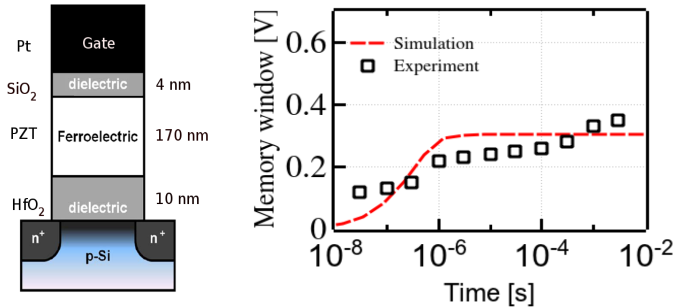

Fig. 9. FE-FET memory window vs. program pulse time for $Si/HfO_2/PZT/SiO_2/Pt$ FE-FET [24]. Increase in measured memory window beyond 1 ms is due to electron injection from gate.

VI. COMPARISON WITH PREVIOUS MODELS

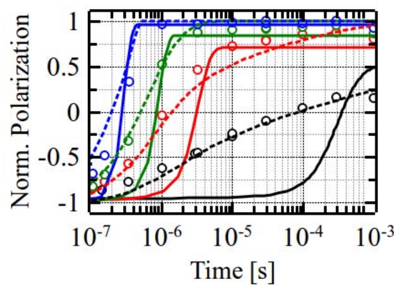

Fig. 10. Simulation of step voltage responses from the time-delayed Preisach model [9] (solid) gives unrealistic results compared to our model (dotted) and experiments (circles)

The Preisach model with time delay in the control parameter [9,10] matches frequency-dependent P-E loops, but not step-voltage polarization responses (Fig. 10). Landau-Khalatnikov circuit models [11] overestimate the coercive field and do not predict kinetics correctly for thermally activated domain switching. None of the previous compact models is applicable to low-field operations, FE with Avrami exponent ≠ 1, FE-FET simulations, or extension to fatigue and imprint modeling.

TABLE I. EXTRACTED PARAMETERS

Parameter	***Symbol***	***Value***
Activation field	E_a	620 kV/cm
Avrami exponent	m	1
Attempt rate: PZT soft phonon frequency	τ_0	10^{-13} s
Nucleation energy exponent	n	1.5
Rayleigh coefficient	γ	44 cm/V
FE electronic dielectric constant	ϵ_{FE}	300
Remanent polarization	P_r	16 $\mu C/cm^2$
Dead layer capacitance	$\mathbf{C_{dead}}$	50 $\mu F/cm^2$

REFERENCES

[1] M. Qazi et al *ISSCC Dig.*, 192-193, (2013).
[2] X. Dong et al, *ACM Trans. Architecture & Code Optimization* (TACO), 8, 2, 6 (2011)
[3] M. Qazi, et al. *IEEE JSSCC,* 47,1, 141-150, (2012)
[4] S Tanakamaru et al,*Proc. IEDM* ,1-4, (2009)
[5] D. El-Damak et al *ISSCC Dig.* , 374-375, (2013)
[6] C.T. Nelson et al, *Science* 334, no. 6058, 968-971, (2011)
[7] A.Q. Jiang et al, *Adv. Func. Mat.* 22, 1, pp. 192-199, (2012)
[8] P.Gao, et al, *Nature comm.* 2, 591, (2011).
[9] E. Supriyanto et al, *Proc. ISAF* 2002, 61-64, (2002)
[10] J. Chow et al, *VLSI Circuits Dig.*, 448-449 (2004)
[11] S. Sivasubramanian et al, *IEEE Trans.Ultra. Ferro. Freq.Cont.*, 50, 8, 950-957 (2003)
[12] W. Merz,*Phys. Rev.* 95, 3, pp. 690, (1954)
[13] R.C. Miller et al,*Phys. Rev.* 117, 1460, (1960)
[14] M.A. Collins et al, *Phys. Rev. B* 19, 3630 (1979)
[15] M. Avrami, *J. Chem. Phys.* 8, 212 (1940)
[16] Y. Ishibashi,Y Takagi,*Journal of Phys. Soc. of Japan* 31, 2, 506-510, (1971)
[17] A.K. Taganstev et al,*Phys. Rev. B* 66, 21, 214109, (2002)
[18] A. Gruverman et al,*App. Phys. Lett.* 87,8, 082902, (2005)
[19] J.Y. Jo et al, *Physical Review Letters* 99, 26, 267602, (2007)
[20] X.J. Lou, *J. Phys.: Condens. Matter* 21 012207, (2009)
[21] M. Vopsaroiu et al, *Phys. Rev. B* 82.2, 024109, (2010)
[22] K.B.Chong et al, *J. Appl. Phys.*, 103, 014101, (2008)
[23] O Boser,*J. Appl. Phys.*, 62, 4, 1344-1348, (1987)
[24] S.R. Rajwade et al,*IEEE Trans. Elec. Dev.* , 60, 6, 1944-1950, (2013)